Supporting Material

A Chemomechanical Model of Matrix and Nuclear Rigidity Regulation of Focal Adhesion Size

Xuan Cao,[1] Yuan Lin,[2] Tristian P. Driscoll,[3] Janusz Franco-Barraza,[4] Edna Cukierman,[4] Robert L. Mauck,[3,5] and Vivek B. Shenoy[1,5,*]

[1]Department of Materials Science and Engineering, School of Engineering and Applied Science, The University of Pennsylvania, Philadelphia, Pennsylvania; [2]Department of Mechanical Engineering, The University of Hong Kong, Hong Kong SAR, China; [3]Department of Orthopaedic Surgery, Perelman School of Medicine, University of Pennsylvania, Philadelphia, Pennsylvania; [4]Cancer Biology Program, Fox Chase Cancer Center, Temple Health, Philadelphia, Pennsylvania; and [5]Department of Bioengineering, School of Engineering and Applied Science, University of Pennsylvania, Philadelphia, Pennsylvania

Experimental Methods

Cell-derived ECM based 3D cultures and indirect immunofluorescence

Cell derived ECMs were obtained as published (1, 2). Briefly, control and desmoplastic fibroblasts were seeded at a confluent cell concentration (i.e., 250,000 cells/ml) onto 0.2% gelatin pre-coated coverslips. Culture media was supplemented with 50 μg/ml ascorbic acid every 24 h during an ECM production period lasting 8 days. ECMs were denuded from cells using an alkaline detergent treatment (0.5% Triton X-100, 20 mM NH4OH in PBS) rendering the assorted ECMs. Naive (i.e., inactivated) fibroblasts were cultured overnight within the assorted ECMs. Cells were fixed/permeabilized as published (1) and indirectly labeled for fibronectin (ECM; in red) or DNA (blue) and alpha5beta1 integrin (3D adhesion structures; in green, monochromatic or digitally highlighted in purple). Images were obtained using a spinning disc confocal microscope with a CFI Apo TIRF 60X Oil objective. Images were acquired at 0.5 μm thick sequential Z planes and a maximum reconstructed projection was provided for the digital imaging analyses using the Offline complete MetaMorph V7.8 software (Molecular Devices, Downingtown, PA). Identical fluorescence intensity thresholds were set for both conditions in order to facilitate adhesion structure selections which were analyzed using the software's integrated morphometric analysis rendering adhesion structure numbers and fiber length of assorted objects (adhesion plaques), expressed in microns. The nuclear shape was determined by calculating the elliptical (Ell) form factor of selected objects (i.e., DNA stained nuclei). *Elliptical Form Factor = length/breadth;* an Ell-FF ratio value of 1 corresponds to a circular shape while numbers greater than 1 represent increasingly elongated nuclear shapes.

Adhesion size depends on nuclear stiffness

To experimentally determine the impact of the nucleus on adhesion size, nuclear connectivity to the cytoskeleton was experimentally perturbed in primary bovine mesenchymal stem cells and adhesion size and number was quantified. For this, knockdown of the LINC complex component nesprin 1 giant was performed using miRNA delivered via lentivirus (Block-it Lentiviral Pol II miR RNAi Expression System with EmGFP, Invitrogen). Three nesprin 1 giant vectors were designed and the miRNA sequence that resulted in the highest levels of knockdown (verified by dot blot for nesprin 1 following 1MDa size filtration) was used (TGCCGAGGACCTTCATCTTCT). Cells were infected with virus overnight, trypsinized 4 days post infection, and re-seeded on glass. The following day, cells seeded on glass slides were fixed and permeablized simultaneously using microtubule stabilizing buffer for 10 minutes at 37°C (0.1M PIPES pH6.75, 1mM EGTA, 1mM $MgSO_4$, 4% w/v polyethylene glycol, 1% Triton X-100, 2% paraformaldehyde), then washed with PBS and stained with anti-vinculin antibody (1:200, Sigma) in 1% w/v BSA in PBS overnight at 4°C. Cells were then washed 3 times with PBS, and then incubated for 60 min at room temperature with Alexa-fluor 546 goat anti-mouse secondary (Molecular Probes, 1:200). Stained cells were washed 3 times and mounted with DAPI containing mounting medium (ProLong Gold Antifade Reagent, Molecular Probes). Images were acquired using a Nikon A1 laser scanning confocal microscope with 20X objective. Z-stacks were acquired at 0.75μm slice thickness over the entire cell with the slice at the base of the cell used for quantification of adhesion size and number. Background subtracted images were converted to binary and adhesions were quantified for each cell (n=7-11 cells per group) using the analyze particles function in ImageJ.

Model descriptions

Boundary conditions for FAs on ECM fibers

As discussed in literature (3, 4), cells are likely to form entire FA on one single fiber *in vivo* as shown in Fig. A1. As actomyosin is pulling the FA to the right, the left side of the ECM fiber is under tension while the right side is under compression. As we know that a fiber of length l under compression would buckle above a critical force (F_{cr}), given by,

$$F_{cr} = \frac{\pi^2 EI}{(Kl)^2} \tag{S1}$$

where E is Young's modulus of the fiber, I is area moment of inertia and K is the column effective length factor. For a typical Collagen-I fibers ($r{\sim}50\ nm$, $l{\sim}30\ \mu m$, $E{\sim}300\ MPa$) (5, 6), from Eq. (S1), the critical buckling force is around 16 pN, which is far smaller than the actomyosin pulling force (around 100 pN) (7). Thus, when a FA forms on the ECM fiber, the right part will buckle, and the fiber provides very small resistance. So for the right boundary is treated as a traction-free edge, or, $du_s/dx|_{x=L} = 0$.

If FA does not start forming at the left edge of the ECM fiber, but from a position at $x = L_l$ (as shown in Fig. A1), this is equivalent to adding a new spring (the stiffness is related to L_l) to the left end of ECM fibers in our existing model. This change would make the effective stiffness (k_{eff}) smaller than the case when FA starts forming at the left end of ECM fiber at a given FA size, but will still show the non-monotonic relation (increasing first then decreasing) with respect to the FA size (L). As a result, our main conclusions will still hold. To better understand the physics and make predictions, we assume that the FA starts forming at the left end of ECM fiber ($L_l = 0$), which allows us to obtain analytical results. Meanwhile, we need to point out that L_l can range from zero to the total length of the fiber. As discussed above, the randomness of this length will result in change in k_{eff} and thus lead to different stable FA sizes. If $L_l = 0$, the stable

size will be the value predicted by our model; if L_l is too large, the stable size will be zero because the local ECM stiffness is too soft for the cell to form FAs at this position. Thus our results provide an upper bound on the FA size.

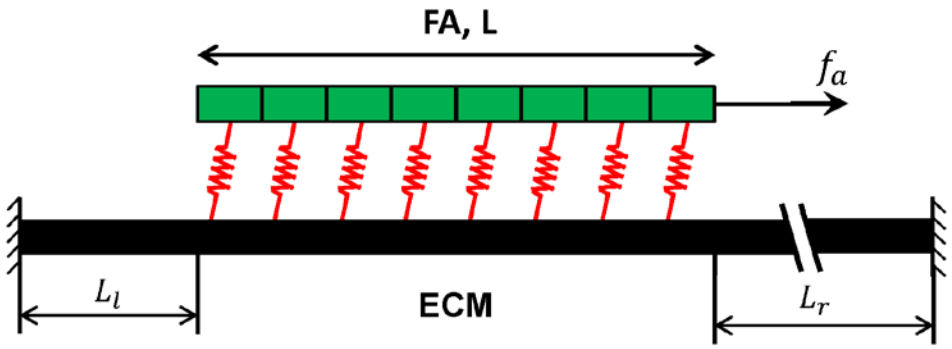

Figure S1: Schematics of FA on an ECM fiber.

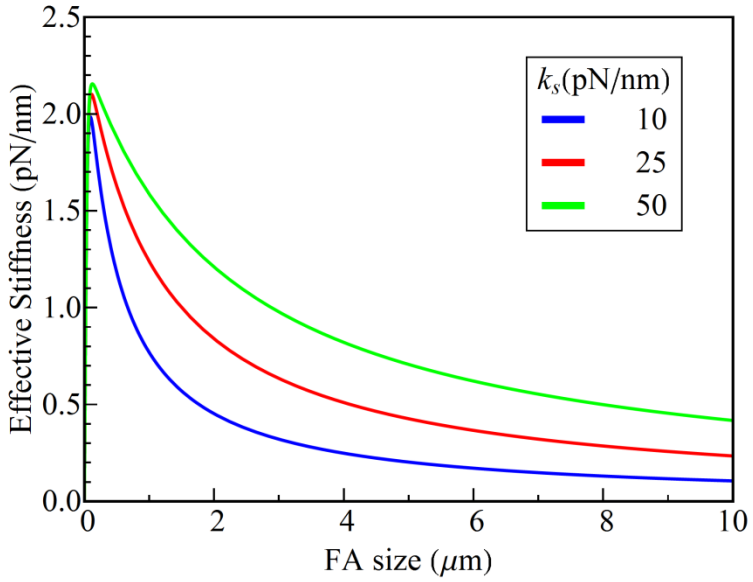

Figure S2: Effective stiffness of FA as a function of FA size and ECM stiffness, plotted in a larger scale.

Governing equations for a continuum representation of the ECM

The equation governing the deformation of the plaque remains the same even if the extracellular side changes from an elastic fiber to a continuous medium, that is

$$k_p d_c^2 \frac{d^2 u_p}{dx^2} = \gamma_c(x) \tag{S2}$$

with $\gamma_c(x)$ being the integrin force at position x which, similar to before, can be expressed as

$$\gamma_c(x) = k_c(u_p(x) - u_s(x)). \tag{S3}$$

To determine the substrate deformation u_s in this case, recall that from the Green's function for an elastic half-space, the surface deflection $u_s^t(x)$ induced by a unit point force at position t is (8)

$$u_s^t(x) = \frac{1+\nu}{\pi E_s}\frac{1}{|x-t|} \tag{S4}$$

where E_s and ν are the Young's modulus and Poisson's ratio of the substrate respectively. By using the principle of superposition, the integrin-force induced substrate displacement can be obtained as

$$u_s(x) = \int_0^L \frac{1+\nu}{\pi E_s}\frac{1}{|x-t|}\gamma_c dt. \tag{S5}$$

Numerical solution of elastic fields with COMSOL

In this study, the finite element package COSMOL was used to solve the problem shown in Fig. 1d. Specifically, a slender elastic fiber and another elastic body, with much larger dimensions, were introduced to represent the adhesion plaque and the substrate, respectively. To simplify the problem, only half of the model was built in COMSOL with symmetric boundary conditions (Fig. S3(a)). These two parts were connected to each other by a series of springs, representing the integrin bonds. During the simulation, a controlled horizontal pulling force was applied on one end of the plaque and the corresponding deformation generated (i.e. the displacement field within the plaque) was then calculated and recorded (refer to Fig. S3(b)), from which the effective stiffness of the FA (defined in Eq. (6)) can be extracted. Results for a denser mesh model are also shown in Fig. S3(b), which provide similar results and indicate that the mesh size used was sufficiently dense.

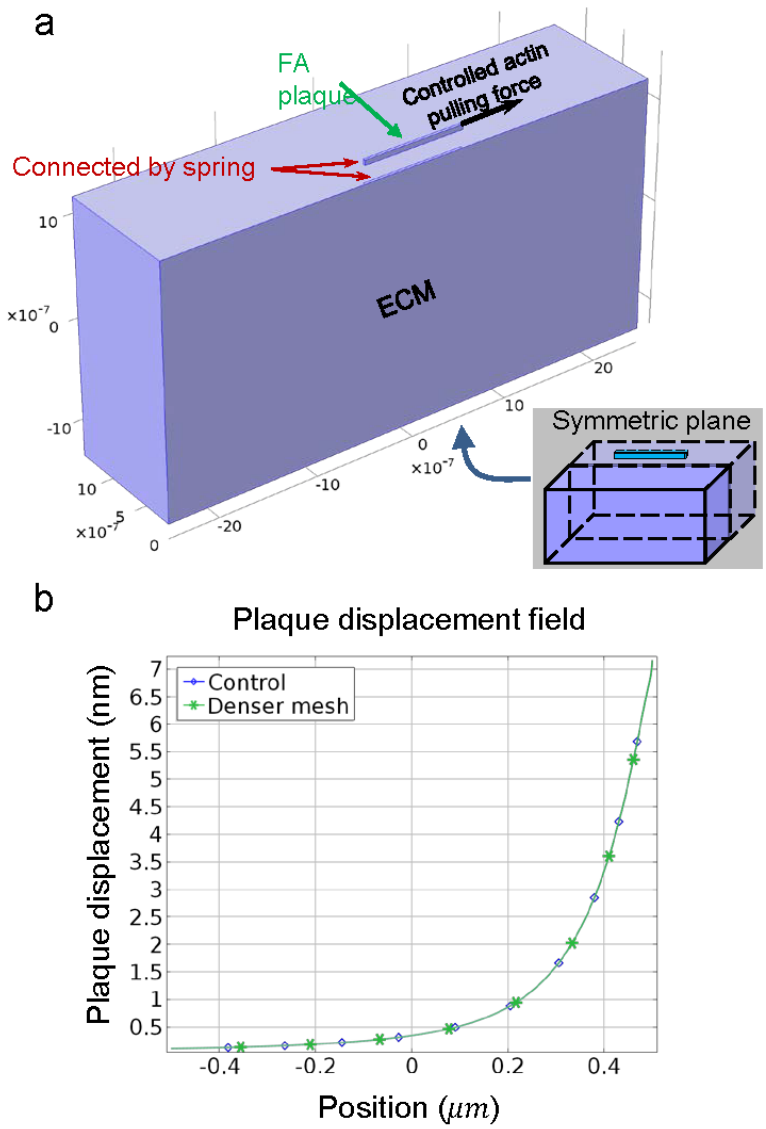

Figure S3: (a) – A computational model built in COMSOL. (b) – A representative simulation result showing the deformation of the plaque with the mesh size used (blue) and a denser mesh (green).

Model predictions

Quantitative comparison between model predictions and experimental results

Note that the rigidities of fibrous ECMs used in our experiments (as shown in Fig. 4) have been measured to be ~7.5 kPa and 5 kPa for the stiff and soft substrates (9), respectively. In addition, the mesh spacing was also observed to be in the range 5 to 15 μm. Relating the fiber stiffness to

the measured modulus and mesh size through the relation, $k_s \approx EL_{mesh}$, yields an effective fiber stiffness of the order of 25-75 pN/nm and 37.5-112.5 pN/nm for the two cases. Using these values and other parameters from Table 1, the stable FA size is predicted to be in the range of 1.8-5.2 μm (median is 3.5 μm) vs 2.7-7.8 μm (median is 5.25 μm) for the soft and the stiff ECMs respectively, which is in good agreement with experimental measurements (3.5 μm vs 5.1 μm for mean FA length as shown in Fig. 4).

Influence of the force distribution acting on the adhesion plaque

To examine whether the distribution of contractile force acting on the adhesion plaque will significantly influence the model predictions, we also considered the case where the force is assumed to be evenly distributed over the whole adhesion plaque .In this case, Eq. 3 should be modified as,

$$\begin{cases} k_p d_c^2 \dfrac{d^2 u_p}{dx^2} = k_c(u_p - u_s) - p \\ k_s d_c^2 \dfrac{d^2 u_s}{dx^2} = -k_c(u_p - u_s) \end{cases}$$

where p represents the force acting on adhesion per unit length. This equation is then solved with similar boundary conditions given in the Section 'METHODS-Model Formulation: Mechanical response of the system', from which the effective stiffness of a FA can be calculated. We find that the effective stiffness first increases and then decreases with respect to the FA size (Fig. S4). In addition, a stiffer ECM also leads to an overall increase of effective stiffness of FAs. Therefore, we do not find any qualitative changes when the nature of the way in which actin force is transmitted through the adhesion plaque is altered.

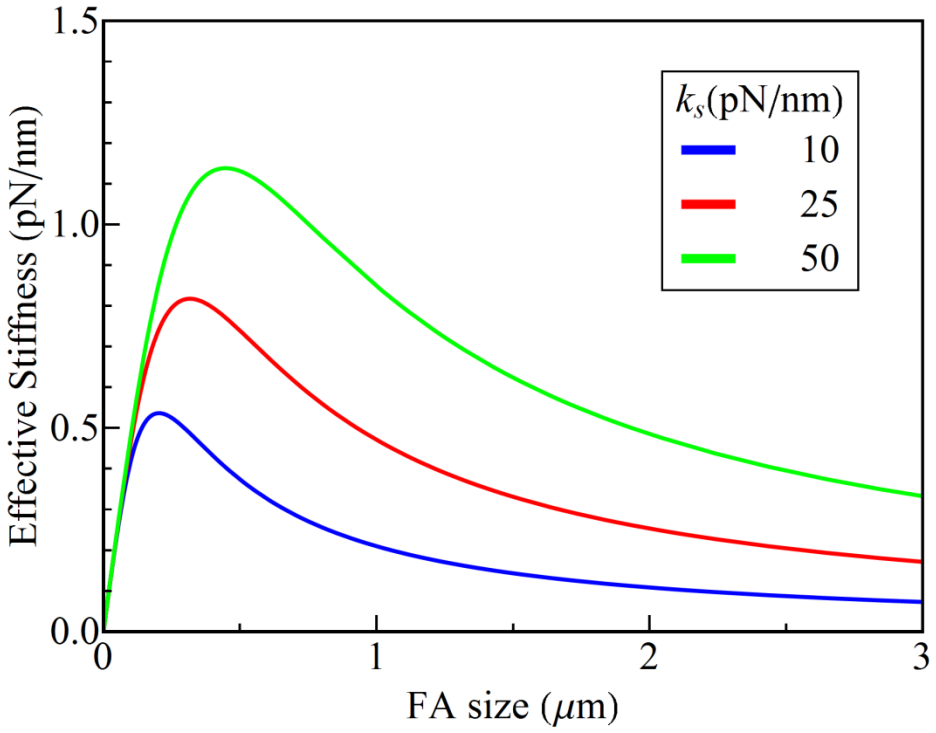

Figure S4: Effective stiffness of a FA as a function of its size and ECM stiffness under the assumption that the contraction force is distributed uniformly across the FA plaque.

Sensitivity of the predictions to model parameters

A parametric study was carried out to demonstrate how our model predictions are influenced by the plaque (Fig. S5a) and integrin stiffnesses (Fig. S5b). Clearly, variations in k_p and k_c will affect the effective stiffness of a FA and eventually change its growth rate. However, the predicted steady-state size of FAs is less sensitive to these variations (they remain with a few micrometers of each other) as shown in the figure below.

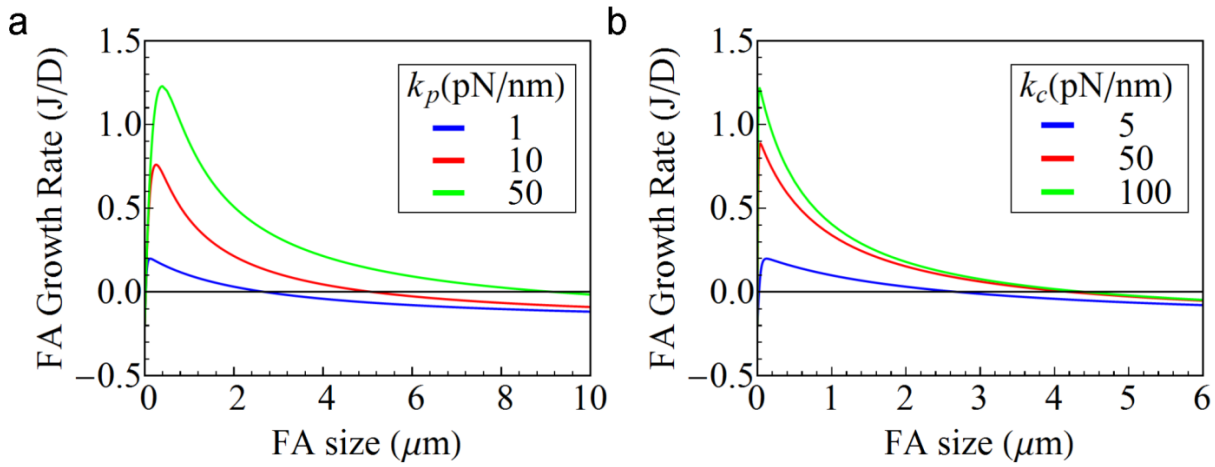

Figure S5: The growth rate of a FA as a function of its size for different plaque (a) and integrin stiffnesses (b).

We have also investigated the dependence of the growth rate – size relationship on the spacing between integrins. Interestingly, as shown in Fig. S6, a larger integrin spacing results in significantly increased critical size, stable size as well as growth rate of FAs, suggesting that it would be harder for the mature adhesions to form. This prediction are consistent with experimental findings that show fewer focal attachments with the ECM when the integrin spacing becomes larger (10).

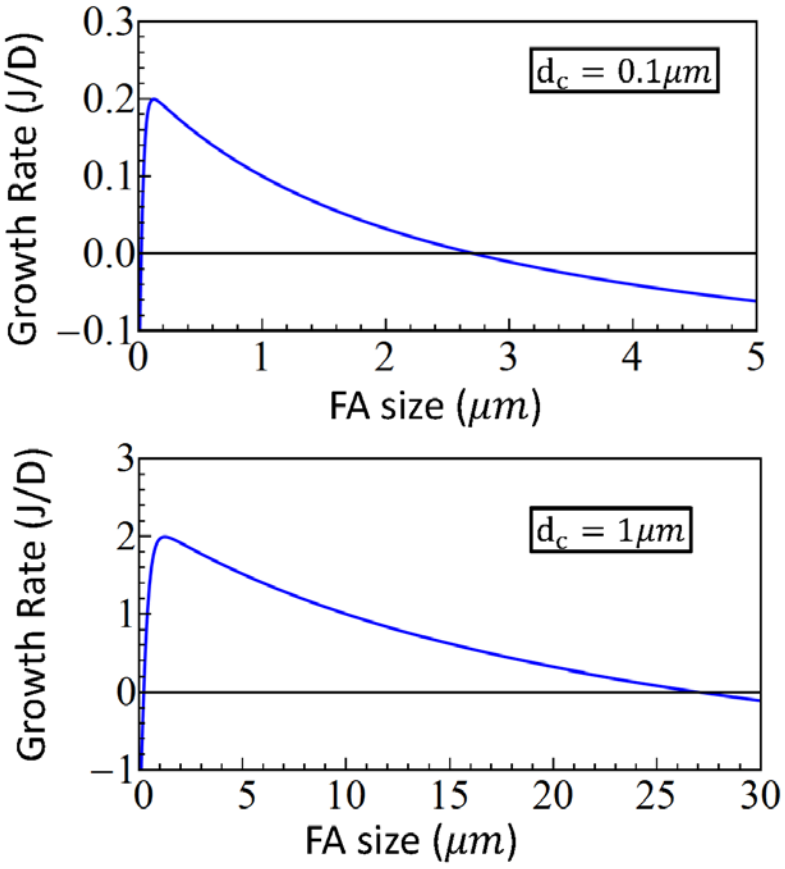

Figure S6: The growth rate – size relationship of FAs for different integrin spacings.

The way that force transmission leads to saturation of k_{eff} when treating the ECM as a continuum elastic medium.

The force distribution among integrin bonds, connecting the adhesion plaque to the elastic half-space (i.e. the ECM) was examined. As shown in Fig. S7, integrins carry the load evenly for small FAs ($L \ll 4L_c$) and hence the force shared by each integrin decreases as more integrins get engaged (i.e. as the FA becomes larger), which results in a smaller deformation of both integrins and the ECM. In this regime, the effective stiffness k_{eff} of a FA increases as it grows. Fig. S7 also demonstrates that the load distribution near the edge of a large FA ($L \gg 4L_c$) actually becomes insensitive to its size (with interior integrin clutches carrying basically zero load).

Given that in this case the actin force is transmitted through an infinite elastic medium (not a 1D fiber with length scale with the FA size), the displacement field in ECM is therefore insensitive to how big the FA is, which corresponds to the saturation value of k_{eff} observed in Fig. 2b.

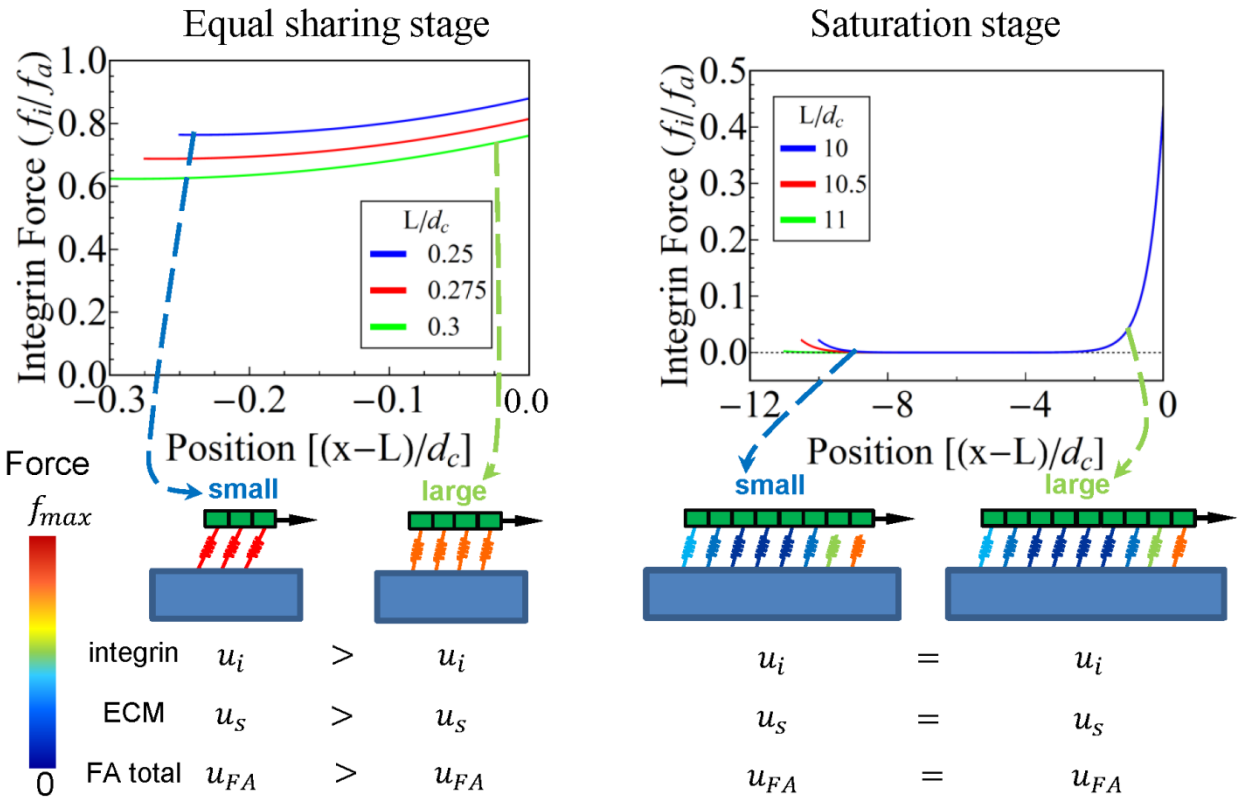

Figure S7: For small FAs ($L \ll 4L_c$), force is almost equally shared by integrins. A larger FA in this regime will lead to lower force on each integrin, resulting in a decreased integrin and ECM displacement at the edge, and hence a monotonic increase of k_{eff}. For very large FAs ($L \gg 4L_c$), integrin force is concentrated in a limited region at their leading edges while the distribution of integrin force is insensitive to FA size. The displacement field of ECM is therefore independent of how big the FA is, leading to a saturated value of k_{eff}. Notice all displacements given here are measured at the right edge (i.e. x=L).

SUPPORTING REFERENCES

1. Castelló-Cros, R., and E. Cukierman. 2009. Stromagenesis during tumorigenesis: characterization of tumor-associated fibroblasts and stroma-derived 3D matrices. Methods Mol. Biol. 522: 275–305.
2. Beacham, D.A., M.D. Amatangelo, and E. Cukierman. 2007. Preparation of extracellular matrices produced by cultured and primary fibroblasts. Curr. Protoc. Cell Biol. Chapter 10: Unit 10.9.
3. Cukierman, E., R. Pankov, D.R. Stevens, and K.M. Yamada. 2001. Taking cell-matrix adhesions to the third dimension. Science. 294: 1708–12.

4. Doyle, A.D., M.L. Kutys, M.A. Conti, K. Matsumoto, R.S. Adelstein, et al. 2012. Micro-environmental control of cell migration--myosin IIA is required for efficient migration in fibrillar environments through control of cell adhesion dynamics. J. Cell Sci. 125: 2244–56.
5. Gentleman, E., A.N. Lay, D.A. Dickerson, E.A. Nauman, G.A. Livesay, et al. 2003. Mechanical characterization of collagen fibers and scaffolds for tissue engineering. Biomaterials. 24: 3805–3813.
6. Matthews, J., G. Wnek, D. Simpson, and G. Bowlin. 2002. Electrospinning of collagen nanofibers. Biomacromolecules. 3: 232–238.
7. Mogilner, A., and G. Oster. 2003. Force generation by actin polymerization II: the elastic ratchet and tethered filaments. Biophys. J. 84: 1591–605.
8. Johnson, K.L. 1985. Contact Mechanics. Aug 28, 19. New York: Cambridge University Press.
9. Goetz, J.G., S. Minguet, I. Navarro-Lérida, J.J. Lazcano, R. Samaniego, et al. 2011. Biomechanical remodeling of the microenvironment by stromal caveolin-1 favors tumor invasion and metastasis. Cell. 146: 148–63.
10. Cavalcanti-Adam, E.A., A. Micoulet, J. Blümmel, J. Auernheimer, H. Kessler, et al. 2006. Lateral spacing of integrin ligands influences cell spreading and focal adhesion assembly. Eur. J. Cell Biol. 85: 219–24.